Title
PROTON-PROTON ELASTIC SCATTERING BETWEEN 6 AND 10 MeV

Authors
Slobodrian, R.J.
Conzett, H.E.
Shield, E.
et al.

Publication Date
1968-05-01

UCRL-18221

cy. 2

University of California

Ernest O. Lawrence Radiation Laboratory

PROTON-PROTON ELASTIC SCATT[illegible]TWEEN 6 AND 10 MeV

[illegible]ERING BE

R. J. Slobodrian, H. E. Conzé[illegible]ld and W. F. Tivol

[illegible], E.

May [illegible]68

Berkeley, California

UCRL-18221
cy. 2

E

DISCLAIMER

To be submitted to: Physical Review

UCRL-18221
Preprint

UNIVERSITY OF CALIFORNIA

Lawrence Radiation Laboratory
Berkeley, California

AEC Contract No. W-7405-eng-48

PROTON-PROTON ELASTIC SCATTERING BETWEEN 6 AND 10 MeV

R. J. Slobodrian, H. E. Conzett, E. Shield and W. F. Tivol

May 1968

PROTON-PROTON ELASTIC SCATTERING BETWEEN 6 AND 10 MeV*

R. J. Slobodrian, H. E. Conzett, E. Shield and W. F. Tivol

Lawrence Radiation Laboratory
University of California
Berkeley, California

May 1968

ABSTRACT

Proton-proton elastic scattering angular distributions have been measured at 6.141, 8.097 and 9.918 MeV laboratory energy, in an experiment designed to achieve an absolute accuracy better than 1%. Phase shift analyses have been performed using S-, split P-, and D-waves. The P-wave splitting was assumed to be dominated by a) a central plus tensor interaction or b) a central plus spin-orbit interaction. In both cases the P-wave splitting was kept small, a condition imposed by the small polarizations measured in this energy range.

* This work was performed under the auspices of the U.S. Atomic Energy Commission.

I. INTRODUCTION

Low energy proton-proton scattering has been the object of very accurate experimental investigation,[1,2] and, except for electromagnetic complications,[2] it is the most suitable source of information concerning the nuclear interaction of two nucleons in the S-wave. The research carried out at Wisconsin was particularly fruitful; two different experimental groups[3,4] covered the range between 1.397 and 4.203 MeV (laboratory energies). Between 4.203 and 10 MeV there have been several other experiments,[5-10] but significant disagreement among these data has indicated the need for more accurate differential cross sections in this energy range.

A comprehensive analysis of the experimental information below 40 MeV was done first by Mac Gregor,[11] using a selection of data in this energy range. The MWF[3] data were the first to show a definite "anomaly" with respect to pure S-wave scattering, and thus indicated the necessity of P-waves in the analysis of low energy p-p cross section data.[12] Early analyses were performed in terms of the S-wave phase shift K_0 and an "effective" P-wave K_1. Mac Gregor[11] stressed the insufficiency of cross section data alone, and his analysis resulted in a four-fold ambiguity among phase shift solutions using S, split P, and D-waves. These solutions predicted different, though small, polarizations, and later measurements[13-15] showed these to be, indeed, small. Thus, large P-wave splittings should be excluded.

One of the interesting aspects of low energy p-p scattering is the possibility of the determination of shape dependent effects on the S-wave phase shift. This is not yet feasible for n-p scattering for which only total cross sections are presently available, and thus even the effective

range parameter is rather inaccurately known.

The ideal region for such a determination is between zero and 10 MeV. An important experiment has been performed in this connection, consisting of the precise determination of the energy of the interference-minimum in p-p scattering.[16] This was measured to be 0.38243 ± 0.00020 MeV, and from this a very accurate value for the $^1S_0$ phase shift was derived.[17] This phase shift, in conjunction with the data of Ref. 4, was used by several authors to attempt a determination of shape dependent parameters in the expression $C^2k \cot g\, \delta_0 + \frac{1}{R} h(\eta) = -\frac{1}{a_p} + \frac{1}{2} r_e k^2 - P r_e^3 k^4 + Q r_e^5 k^6 - \ldots$, where the symbols have the usual meaning.[18] Reference 18 contains a summary of the situation concerning this point. There are uncertainties if the analysis is restricted to the interference minimum datum and to the KMBND[4] data set. The inclusion of the WMF data in the analysis reduces such uncertainties,[18] but, nevertheless, the shape dependent scattering parameters are not determined unambiguously. Heller[2] has recently added the phase shift at 9.69 MeV, obtained from the data of Johnston and Young,[10] to the interference minimum datum and to the KMBND data set. The analysis was carried out using the effective-range expansion up to and including a cubic term in the energy. The shape dependent coefficients P and Q were obtained with large errors. It is also well known that the point at 9.69 MeV is too close to the radius of convergence of the series to warrant a fit with a small number of terms in the expansion. This was recognized by Heller himself.

Another approach was made recently by Noyes and Lipinski[19] in analyzing the 9.69 MeV data[10] and incorporating in the analysis a ratio of spin-orbit to tensor effects; higher partial waves were calculated in terms of a model.

Vacuum polarization and electromagnetic structure effects in the S-wave were neglected. They concluded that the $^1S_0$ phase shift determined in the analysis was in modest agreement with the predicted OPE shape correction.

The measurement of precise angular distributions between 4.203 and 10 MeV to better than 1% absolute accuracy seemed to be another promising angle of attack to solve the problem of shape dependence.[20] Another paper[21] will describe the determination of the shape dependent parameters P and Q from the interference minimum phase shift, the WMF data, the KMBND data and the results reported here.

II. EXPERIMENTAL DETAILS

A. Scattering Chamber, Beam Energy and Charge Collection

The Berkeley 88-inch sector-focused cyclotron was used to produce a proton beam, accelerated as H_2^+ ions. The reason for this was twofold: slit scattered H_2^+ ions result in free protons that are not focused by the beam transport system, and thus slit effects are minimized. It was also a means of reaching the low energies required in this experiment. The beam was conveyed through an analyzing magnet and quadrupole magnet lenses into the scattering chamber. The beam was defined by nickel slits and carbon antiscattering baffles. The entrance foil was 0.25 mil thick dural, and the exit foil was about 3" diameter, 1.9 mil thick. Figure 1 shows the general layout of the scattering chamber. The pressure was measured to $\pm$ 0.1% accuracy with absolute silicon oil manometers. It was continuously monitored via a closed circuit television system with cameras sighting both ends of the silicon oil columns. Calibrations of this manometer were made by measuring the oil density relative to both

distilled water and distilled mercury. The results of such alternative methods agreed to one part in 10^4. Precision thermometers were placed on the body of the scattering chamber and on the silicon oil manometers, contact was effected with silicon grease. The temperature was measured to ± 0.1°K and the total variation of it throughout the experiment was within ± 0.25°. The experimental cave is isolated from the outside with thick concrete blocks and its temperature remained very stable, particularly since care was exercised in restricting the opening of the heavy concrete door. The collection of charge was done with a Faraday cup and an integrating electrometer, accurate to ± 0.1%. Calibrations were performed before, during, and after the experiment using the electric current method with resistors and voltages measured to one part in 10^4. The current calibrations were performed at different intensities covering the range used during the experiment. During the calibration, the box containing resistors was kept at constant temperature. A thermometer accurate to 0.1°K was used to monitor the temperature. The integrating circuit capacitor was insensitive to the small temperature changes which occurred during the experiment, within ± 0.2°K. The beam integrator contained a fast relay for the recycling of the integrator circuit. The correction for its dead time was readily determined using the current method at the intensities employed during the experiment. The maximum correction was (2 ± 0.1)%.

The beam energy was determined through its range in aluminum, and converted using experimental ranges.[22] Energies at the center of the target were 6.141, 8.097, and 9.918 MeV, with target gas pressure near 0.050, 0.075, and 0.1 atmospheres, respectively. The range-energy conversion is accurate to about ± 0.1%. Thus, a limit of error on the energy determination can be

safely set at ± 0.4%, which includes some small drifts of the beam energy during the experiment.

The width at half maximum of forward angle spectra was 63 keV at 9.918 MeV, 50 keV at 8.097 MeV, and 59 keV at 6.141 MeV, mainly due to the energy resolution of the detectors, electronic noise and gas geometry. The beam width itself was below 10 keV. The detector collimators were constructed with brass and slits were cut on 11 mil thick nickel plate. Rectangular geometry was used and the alignment was effected optically with a transit. The collimator assembly was provided with fine thread screw adjustments, permitting an accuracy close to one mil in the horizontal plane alignment. The vertical adjustment was, of course, less critical but it was achieved with a comparable accuracy. The angular resolution was 0.5°. The detector arms were aligned optically, and the position was read on two dials with vernier scales. The coupling of the arms to the dials was rigid, and there was no uncertainty usually associated with indirect readouts or non rigid couplings

The measurement of distances from the center of the chamber to the collimators was performed to an accuracy better than one part in 10^4 for most linear dimensions. The slits themselves were measured with a very precise optical comparator system, equipped with a digital readout. The accuracy of this apparatus was ± 0.1μ. The slits were in the range of 1500μ wide and were mapped at about 150μ intervals. Both faces of the slit were mapped and a slight wedging was determined. The areas of the rear slits were evaluated by numerical integration of the mapping. The front slit width was averaged over the utilized section as determined by the finite beam size.

B. Detection and Electronics

Detection of scattered protons was accomplished with two lithium drifted silicon detectors, one on either side of the beam. The positioning of detector assemblies was accurate to 0.016°. A single collimation geometry was used at all angles with a value of about 7×10^{-6} cm-sr. This choice had, of course, advantages in that it eliminated normalization errors that could occur if several geometries had been used. Counting rates were kept constant by changing the beam intensity as a function of angle.

Counting statistics were kept in the range of 0.3%. Dead time losses were kept below 1% and corrected by means of fast scalers to ± 0.1% accuracy. Figure 2 shows a diagram of the electronics. Spectra were stored in two pulse-height analyzers. Two monitor detectors were also used, one at 8° and the other at 25°, off the horizontal plane. Their spectra were also recorded in an analyzer.

Coincidences (prompt and delayed) between both detectors in the horizontal plane were also recorded in order to obtain an indication of inelastic events. The net difference between real and accidental coincidences set a limit on inelastic events at about 0.1% of the elastic cross sections.

Tests of the beam alignment were made by interchanging positions of the detector assemblies. The two independent yields were in agreement within the statistical fluctuation and the contribution due to the angular positioning error. Scalers were used in duplicate since their accurate numbers were necessary to correct for dead time losses in the pulse-height spectra.

III. EXPERIMENTAL CROSS SECTIONS AND ERRORS

Spectra were measured between 6° and 50° in the laboratory system. Figure 3 shows a typical experimental spectrum at a small angle. Some discussion is appropriate concerning the evaluation of counts under the peak. The technique used for the Wisconsin experiments,[3,4] performed with gaseous proportional counters, relied on a discriminator method applied on a ΔE spectrum (ΔE is a small fraction of the energy of the protons entering the sensitive volume of the detector). The series of experiments of Johnston and collaborators[10] at Minnesota was performed with NaI (Tl) scintillators, the protons stopped in the crystal producing a signal proportional to energy. However, the energy spectrum was mainly used for the purpose of setting a discriminator at a certain level below the peak, and the peak integration was performed using fast scalers counting all pulses above the discriminator setting. Such pulses were assumed to be "elastically" scattered protons.

We have consistently recorded the energy spectra at all measured angles. The small peak due to elastic scattering on impurities separates well from the elastic proton-hydrogen peak at angles larger than 7° (laboratory system). For consistency with the "discriminator methods" used in the experiments mentioned above we have evaluated the peak counts by means of the simulation of a discriminator setting (from now on called D data). However, if a "background" line is extrapolated from the spectrum shape at energies below the peak, the cross section values are reduced between 0.5 and 1%. Therefore, we have also determined cross sections using a background subtraction method (from now on called BGS data).

A summary of typical errors is given in Table I. The errors at the two smallest angles of Table II are largely due to the uncertainty in the subtraction of the elastic peak of contaminants. The yield due to contaminants was consistent with the quoted purity of H_2 gas at the beginning of the experiment at each energy. The build up of contaminant was rather slow and increased from 0.01% to 0.05% during the measurement of each angular distribution. This was determined by evaluation of the impurity peak counts on the monitor detector at 25°. The small angles were measured first with new gas. At larger angles the elastic group of protons scattered off hydrogen would separate from the contaminant peak. The contribution from inelastic scattering to excited states of the contaminants in the investigated angular range was less than 0.1% of the elastic scattering off hydrogen. It was not deemed necessary to renew the gas during the experiment at a given energy, nor to use a flow system in view of the exceptional vacuum tightness of the scattering chamber. Wall outgassing was probably the major contribution to the small contaminant build up.

The simultaneous measurement of yield on both sides of the beam permitted a considerable reduction in the errors from possible misalignment of the beam. The number of yield measurements was larger than 100, and only two were finally discarded from the analysis. The accuracy of the fast scalers was measured with a pulse generator at the rates used during the experiment, and it was found to be better than 0.1%. Dead time corrections exhibited a reasonable consistency for both detector systems.

Table II summarizes the cross sections obtained with the background subtraction technique and also with the discriminator method. Second order

geometry corrections were calculated using formulas developed by Silverstein.[23] Finite beam and divergence effects were calculated numerically, and the resulting corrections were necessary only at small angles. Corrections for slit effects and multiple-scattering were made following the experience of the measurements performed at Wisconsin, using formulas for multiple scattering due to Williams[24] and Molliere.[25] The detection efficiency of the solid state detectors is close to unity in the energy range between 0 and 10 MeV. However, the loss due to reactions was corrected approximately using recent experimental results and calculations.[26] The conversion of cross sections to the center-of-mass system was accomplished using the appropriate relativistic Jacobian transformation.

IV. ANALYSIS

A phase shift analysis was performed using a program developed by Knecht[27] and written by Jenkins. It was adapted for use with a CDC 6600 computer. This program includes S, P and D-waves. The conclusions reached by Noyes and Lipinski[19] at 9.69 MeV concerning the negligible contribution of F-waves are also applicable at 9.918 MeV, and, a fortiore, they hold at lower energies. Also, the results of recent phenomenological phase-parameter fits by the Yale group[28] show negligible F-wave contributions at 10 MeV. Consequently, we have considered that an analysis limited to S, P and D-waves is valid and meaningful for experiments of the order of 0.5 to 1% accuracy. Vacuum polarization corrections for $\ell = 1$ were carried out using formulae derived by Durand.[29] The S-wave vacuum polarization correction was not performed, as it is easily done using the procedure of Foldy and Eriksen[30] in the effective range expansion.

Noyes and Lipinski[19] have concluded that the $^3P_{0,1,2}$ phase shifts $\delta_{1,J}$ should have the + - + OPE signature at 9.69 MeV and that Δ_{LS}/Δ_T should be in the range 0.07 to 0.15 where

$$\Delta_{LS} = (-2\,\delta_{1,0} - 3\,\delta_{1,1} + 5\,\delta_{1,2})/12$$

and

$$\Delta_T = 5(2\,\delta_{1,0} - 3\,\delta_{1,1} + \delta_{1,2})/72$$

Nevertheless, following a more phenomenological approach we have chosen in our analysis to retain the possibility of two different signatures of the split P-wave phase shifts. One is consistent with a tensor interaction producing negative polarizations, while the other (+ + - signature), produces a positive polarization at small angles and corresponds to a dominant spin-orbit interaction. In both cases the strength of the splitting was kept small, consistent with the existing experimental values of polarization.[13,14]

Results of our analysis are given in Tables III-VI. The listed errors are based on the criterion of an increase of 1 in χ^2, and, alternatively, in the parameter $\Phi = \chi^2/N$ (where N is the number of data points). The program adjusts the S-wave, the central force part of the P-wave and the D-wave phase-shifts in successive steps. Table VII shows the values obtained for the S-wave phase shift at each step.

Figure 4 contains a plot of the angular distributions of D data obtained in our experiments, together with those obtained by other groups at neighboring energies. Figure 5 shows an excitation function of the cross section at 20° and 90° CM utilizing data from several sources. Figure 6 contains a plot of the $^1S_0$ shifts obtained from our D data and from other

sources. Included are some recent values calculated by Mac Gregor et al.[31] as a reasonable extrapolation to low energies from analysis of higher energy data. However, these low energy values were obtained in the context of a shape independent approximation and therefore comparison with experiment may be rather unfavorable. The phase shifts obtained by Seamon et al.[28] at 10 and 20 MeV are also plotted; in our opinion they agree better with experiment than the values of Ref. 31 at energies between 10 MeV and 30 MeV.

Our cross sections at 9.918 MeV disagree with the extrapolated values obtained from the Minnesota experiment at 9.69 MeV, assuming a 1/E dependence of the cross section, by more than one standard deviation. The plot of the excitation functions in Fig. 5 is not expanded enough to show this difference but the plot of phase shifts in Fig. 6 bears this out. However, the cross sections measured at Minnesota are on the order of 1 to 2% higher than the values obtained at the Rutherford high energy laboratory,[33] at the energies where they overlap. Mac Gregor et al. assign a probable normalization of 1.015 to the final search in fitting the data, this means that the data should be scaled by 0.985 for consistency with their phase shift solution. Figure 7 shows the polarizations calculated from our phase shifts with the two different P-wave splittings.

V. FINAL REMARKS

Figure 6 shows that the information reported in this paper maps the region of the maximum of the p-p $^1S_0$ phase shift. It indicates that there is some need for measurements in smaller energy steps both below 10 MeV and between 10 and 20 MeV. One of the problems that has plagued the field above the van de Graaf region covered by the Wisconsin experiments has been the availability of single energy machines, and therefore data have been produced in the course of time with different techniques, energy spread and beam stability. Presently the much higher energy range of electrostatic generators as well as the variable energy feature of cyclotrons allow a broad energy range to be covered by the same experimental group. This is the natural evolution of the art, and its importance is obvious. Data acquisition techniques have advanced very far at present, and it is possible to perform accurate work in the measurement of small polarizations, spin correlations, etc.

Another aspect still requiring attention and more thorough investigation is that of bremsstrahlung effects. They probably originate in transitions involving mainly the P-wave, and therefore, although such effects are small, they may be relevant to a more exact formulation of the scattering amplitude, assumed to be purely elastic below the meson production threshold. Precise measurements have been repeatedly advocated, as they may provide a means for distinguishing between nucleon-nucleon potentials fitted to elastic scattering data.[34]

ACKNOWLEDGMENTS

We are thankful to Prof. H. Pierre Noyes, L. H. Johnston, Drs. M. H. Mac Gregor and D. J. Knecht for useful discussions and/or kindly providing preprints of their work prior to publication. It is also a pleasure to thank Prof. Gregory Breit, who indirectly was very helpful in the development of this work.

These experiments could not have been accomplished successfully without the high quality support of the technical staff of the 88" cyclotron and LRL. We thank particularly T. Chan for designs of mechanical parts, John Meneghetti for supervising their construction, assembly and also for useful suggestions, B. Lothrop for providing excellent Si detectors, and D. Landis for his support with the electronic equipment.

REFERENCES

1. A summary of work prior to 1950 is contained in J. D. Jackson and J. M. Blatt, Rev. Mod. Phys. 22, 77 (1950).
2. L. Heller, Rev. Mod. Phys. 39, 584 (1967) and references therein.
3. H. R. Worthington, J. N. Mc Gruer and E. D. Findley, Phys. Rev. 90, 899 (1953), referred to as WMF.
4. D. J. Knecht, S. Messelt, E. D. Berners and L. C. Northcliffe, Phys. Rev. 114, 550 (1959); D. J. Knecht, P. F. Dahl, and S. Messelt, Phys. Rev. 148, 1031 (1966), referred to as KMBND.
5. James Rouvina, Phys. Rev. 81, 593 (1951).
6. K. B. Mather, Phys. Rev. 82, 133 (1951).
7. J. C. Allred, A. H. Armstrong, R. O. Bondelid, and L. Rosen, Phys. Rev. 88, 433 (1952).
8. E. J. Zimmermann, R. O. Kerman, S. Singer, P. Geral Kruger, and W. Jentschke, Phys. Rev. 96, 1322 (1954).
9. B. Cork and W. Hartsough, Phys. Rev. 94, 1300 (1954).
10. L. H. Johnston and D. E. Young, Phys. Rev. 116, 989 (1959).
11. M. H. Mac Gregor, Phys. Rev. 113, 1559 (1959).
12. H. H. Hall and J. L. Powell, Phys. Rev. 90, 912 (1953).
13. J. Alexeff and W. Halberli, Nucl. Phys. 15, 609 (1960).
14. R. J. Slobodrian, J. S. C. Mc Kee, H. Bichsel and W. F. Tivol, Phys. Rev. Letters 19, 704 (1967) and references therein.
15. P. Catillon, J. Sura and A. Tarrats, Phys. Rev. Letters 20, 602 (1968).
16. J. E. Brolley, Jr., J. D. Seagrave, and J. G. Berry, Phys. Rev. 135, B1119 (1964).

17. M. L. Gursky and L. Heller, Phys. Rev. 136, B1693 (1964).

18. R. J. Slobodrian, Nucl. Phys. 85, 33 (1966) and references therein.

19. H. Pierre Noyes and L. Lipinski, Phys. Rev. 162, 884 (1967).

20. R. J. Slobodrian, H. E. Conzett, E. Shield and W. F. Tivol, Proceedings of the International Nuclear Physics Conference at Gatlinburg (1966) (Academic Press, New York).

21. R. J. Slobodrian, UCRL-18223 (unpublished) and to be published.

22. H. Bichsel, R. F. Mozley, and W. F. Aron, Phys. Rev. 105, 1788 (1957); H. Bichsel, Phys. Rev. 112, 1089 (1958).

23. E. A. Silverstein, Nuclear Instr. 4, 53 (1959).

24. E. J. Williams, Phys. Rev. 58, 292 (1940).

25. G. Molliere, Z. Naturforsch. 3a, 78 (1948).

26. J. J. Kraushaar, R. A. Ristinen, R. Smythe, Phys. Letters 25B, 13 (1967); M. Q. Makino, C. N. Wadell, and R. M. Eisberg, Nuclear Inst. 60, 109 (1968).

27. D. J. Knecht, Technical Documentary Report No. WLTDR-64-78 (1964) (unpublished).

28. R. E. Seamon, K. A. Friedman, G. Breit, R. D. Haracz, J. M. Holt, and A. Prakash, Phys. Rev. 165, 1579 (1968).

29. L. Durand III, Phys. Rev. 108, 1597 (1957).

30. L. L. Foldy and E. Eriksen, Phys. Rev. 98, 775 (1955); M. de Wit and L. Durand, Phys. Rev. 111, 1597 (1958).

31. M. H. Mac Gregor, R. A. Arndt, and R. M. Wright, UCRL-70075 (Part VII) (unpublished and to be published).

32. We have reanalyzed the Minnesota cross sections to avoid systematic differences that may stem from the analysis. We agree within error with the values of Ref. 17.

33. C. J. Batty, R. S. Gilmore, and G. H. Stafford, Nucl. Physics 41, 388 (1963); C. J. Batty, G. H. Stafford, and R. S. Gilmore, loc. cit. 51, 255 (1964).

34. V. B. Brown, Phys. Letters 25, 506 (1967) and references therein.

35. S. Kikuchi, J. Sanada, S. Suwa, I. Hayashi, K. Kisimura, and K. Fukunaga, Jour. Phys. Soc. Japan 15, 9 (1960).

36. J. L. Yntema and M. G. White, Phys. Rev. 95, 1226 (1954).

37. J. Burkig, D. Shrank, and J. R. Richardson, Phys. Rev. 100, 1805 (1959).

38. L. H. Johnston and Y. S. Tsai, Phys. Rev. 115, 1293 (1959).

39. V. E. Kruse, J. M. Teem, and N. F. Ramsey, Phys. Rev. 101, 1079 (1956).

40. S. I. Bile'kaya, Yu. M. Kazarinov, F. Lehar, and Z. Janout, Yadern. Fiz. 4, 892 (1966)[translation: Soviet J. Nucl. Phys. 4, 635 (1967)].

41. C. J. Batty and J. K. Perring, Phys. Letters 16, 301 (1965).

FIGURE CAPTIONS

Fig. 1. Layout of the scattering chamber (not to scale).

Fig. 2. Schematic of the electronics.

Fig. 3. Sample spectrum at 6° Lab and 9.918 MeV.

Fig. 4. Angular distributions in p-p scattering. The solid circles were measured in the present set of experiments. The squares were taken from Ref. 3. The triangles (open and solid) were taken from Ref. 8. The open circles were measured by Johnston and Young, Ref. 10.

Fig. 5. Excitation functions of p-p differential cross sections at 20° and 90° CM. The open circles were taken from Refs. 3 and 4. The upright triangles were measured in the present set of experiments; the squares are from Ref. 8; the inverted triangles are from Refs. 10 and 38 the diagonal cross is from Ref. 7; the encircled straight cross is from Ref. 9; the double circles are from Ref. 35; the straight cross is from Ref. 36; the encircled diagonal crosses are from Ref. 37; the asterisks are from Ref. 39; the solid dot from Ref. 39.

Fig. 6. $^1S_0$ phase shifts. Solid squares were obtained with the data of Refs. 3 and 4. Inverted solid triangles are from Ref. 8. The open upright triangles are the solution from Ref. 31, the inverted open triangles are from Ref. 28, the solid dots were obtained with D data and OPE P-wave splitting in our experiments; the open circle is obtained from the data of Ref. 10; the open diamond comes from Ref. 35; the open squares are two values obtained by Ref. 40; and the solid triangles were obtained by Ref. 41.

Fig. 7. Angular distributions of polarizations obtained with the P-wave spin orbit splitting (solid line) and the OPE splitting (dashed line).

a) 6.141 MeV.

b) 8.097 MeV.

c) 9.918 MeV.

Table I. Typical errors.

SOURCE	ERROR ±(%)
Charge collection	0.1
Statistics	0.3
Gas pressure	0.1
Gas temperature	0.05
Geometry factor	0.1
Scaler tracking	<0.1
Chamber empty background	<0.1
Nuclear reactions (detector efficiency)	0.1
Extrapolated background	0.5 - 1.0
Alignment	0.1
Combined	0.6 - 1.07

Table II. Experimental cross sections.

E_{LAB} [MeV] / θ_L (degrees)	6.141 C.M. Cross Sections $d\sigma/d\Omega$[mb·sr^{-1}] BGS	6.141 C.M. Cross Sections $d\sigma/d\Omega$[mb·sr^{-1}] D	8.097 C.M. Cross Sections $d\sigma/d\Omega$[mb·sr^{-1}] BGS	8.097 C.M. Cross Sections $d\sigma/d\Omega$[mb·sr^{-1}] D	9.918 C.M. Cross Sections $d\sigma/d\Omega$[mb·sr^{-1}] BGS	9.918 C.M. Cross Sections $d\sigma/d\Omega$[mb·sr^{-1}] D
6	976.35±30.07	989.53±30.48	564.06±16.92	571.05±17.13	386.16±3.86	390.07±3.90
7	516.26±16.62	526.01±16.62	318.82± 6.38	322.13± 6.44	213.47±2.29	215.47±2.31
8	309.71± 9.97	313.00± 9.11	191.16± 1.45	193.06± 1.47	132.28±0.91	133.60±0.92
9	213.00± 5.86	214.77± 5.91	131.26± 0.72	132.13± 0.73	94.14±0.75	95.11±0.76
10	152.79± 1.02	154.00± 1.02	98.61± 0.66	99.43± 0.66	73.39±0.61	74.20±0.62
11	121.74± 0.70	122.54± 0.71	82.02± 0.50	82.64± 0.51	61.99±0.54	62.71±0.54
12	103.40± 0.55	104.00± 0.55	72.82± 0.49	73.44± 0.50	55.83±0.40	56.34±0.40
14	85.74± 0.45	86.21± 0.45	63.41± 0.41	63.91± 0.41	50.86±0.28	51.17±0.28
16	80.52± 0.42	80.97± 0.43	61.67± 0.42	62.19± 0.42	48.97±0.27	49.30±0.27
18	78.89± 0.39	79.29± 0.39	60.83± 0.39	61.31± 0.39	49.48±0.22	49.72±0.22
20	78.99± 0.40	79.41± 0.40	61.08± 0.38	61.55± 0.38	49.74±0.33	50.13±0.33
25	80.70± 0.38	81.06± 0.38	62.43± 0.33	62.92± 0.33	50.16±0.39	50.64±0.39
30	81.94± 0.33	82.20± 0.34	63.25± 0.41	63.77± 0.42	50.80±0.43	51.35±0.43
35	82.74± 0.39	83.12± 0.39	63.52± 0.42	64.03± 0.42	51.43±0.47	52.02±0.48
40	82.95± 0.50	83.51± 0.50	63.92± 0.54	64.61± 0.55	52.05±0.50	52.70±0.50
45	82.93± 0.91	84.00± 0.92	64.92± 0.55	65.93± 0.56	52.49±0.56	53.22±0.56
50	83.54± 1.44	85.47± 1.47	---	---	51.31±0.99	52.66±1.01

Table III. Results of the phase shift analysis of BGS data assuming a P-wave splitting consistent with OPE. Columns labeled σ correspond to an increase of 1 in χ^2, and τ to an increase of 1 in Φ.

E_{LAB}	χ^2	Phase Shifts [degrees]											
MeV		$^1S_0$	σ_s ±	τ_s ±	$^3P_0$	$^3P_1$	$^3P_2$	σ_P ±	τ_P ±	$^1D_2$	σ_D ±	τ_D ±	
6.141	5.13	55.54	0.024	0.102	2.36	-1.24	0.196	0.029	0.126	0.116	0.131	0.564	
8.097	9.82	55.63	0.024	0.120	3.16	-1.64	0.282	0.049	0.243	0.118	0.124	0.619	
9.918	10.34	54.78	0.032	0.167	3.88	-2.12	0.276	0.094	0.489	0.105	0.204	1.049	

UCRL-18221

Table IV. Results of the phase shift analysis of BGS data assuming a P-wave splitting dominated by spin-orbit effects producing a positive and small polarization for angles smaller than 15° .

E_{LAB}	χ^2	Phase Shift [degrees]											
MeV		$^1S_0$	σ_s ±	τ_s ±	$^3P_0$	$^3P_1$	$^3P_2$	σ_P ±	τ_P ±	$^1D_2$	σ_D ±	τ_D ±
6.141	5.14	55.35	0.0253	0.1093	1.38	1.62	-1.39	0.0372	0.161	0.173	0.136	0.587
8.097	9.83	55.11	0.0245	0.1225	2.09	2.46	-2.12	0.0483	0.242	0.245	0.129	0.647
9.918	10.34	53.75	0.0357	0.1839	2.72	3.21	-2.98	0.113	0.582	0.344	0.318	1.640

Table V. Results of the phase shift analysis of D- data assuming a P-wave splitting consistent with OPE. Columns labeled σ correspond to an increase of 1 in χ^2, and τ to an increase of 1 in Φ.

E_{LAB}	χ^2	Phase Shift [degrees]											
MeV		$^1S_0$	σ_s ±	τ_s ±	$^3P_0$	$^3P_1$	$^3P_2$	σ_P ±	τ_P ±	$^1D_2$	σ_D ±	τ_D ±
6.141	5.56	55.67	0.025	0.109	2.317	-1.283	0.157	0.038	0.168	0.075	0.130	0.576
8.097	13.68	55.91	0.021	0.114	3.135	-1.665	0.255	0.050	0.271	0.067	0.126	0.686
9.918	9.37	55.09	0.031	0.159	3.826	-2.174	0.226	0.106	0.532	0.009	0.230	1.154

Table VI. Results of the phase shift analysis of D data assuming a P-wave splitting dominated by spin-orbit effects producing a small positive polarization for angles smaller than 15°. Columns labeled σ correspond to an increase of 1 in χ^2 and τ to an increase of 1 in Φ.

E_{LAB}	χ^2	Phase Shift [degrees]											
MeV		$^1S_0$	σ_s ±	τ_s ±	$^3P_0$	$^3P_1$	$^3P_2$	σ_P ±	τ_P ±	$^1D_2$	σ_D ±	τ_D ±
6.141	5.57	55.49	0.025	0.112	1.344	1.584	-1.435	0.038	0.166	0.133	0.137	0.605
8.097	13.69	55.40	0.024	0.133	2.060	2.429	-2.144	0.050	0.271	0.198	0.130	0.708
9.918	9.39	54.05	0.021	0.107	2.665	3.165	-3.035	0.121	0.601	0.249	0.324	1.630

Table VII. Phase shifts for the analysis minimizing χ^2 and varying the S-wave phase shift, S and P-wave phase shifts and S, P, and D-wave phase shifts.

S-Wave Phase Shifts

E_{LAB} \ Phase Shifts Varied	Discriminator Data			Background Subtracted Data		
	S	S,P	S,P,D	S	S,P	S,P,D
	OPE Splitting					
6.141	55.84	55.68	55.68	55.64	55.52	55.54
8.097	56.03	55.91	55.91	55.71	55.62	55.63
9.918	55.28	54.95	55.09	54.97	54.72	54.78
	SO Splitting					
6.141	55.76	55.47	55.49	55.56	55.31	55.35
8.097	55.81	55.40	55.40	55.49	55.12	55.11
9.918	54.91	54.09	54.05	54.60	53.86	53.75

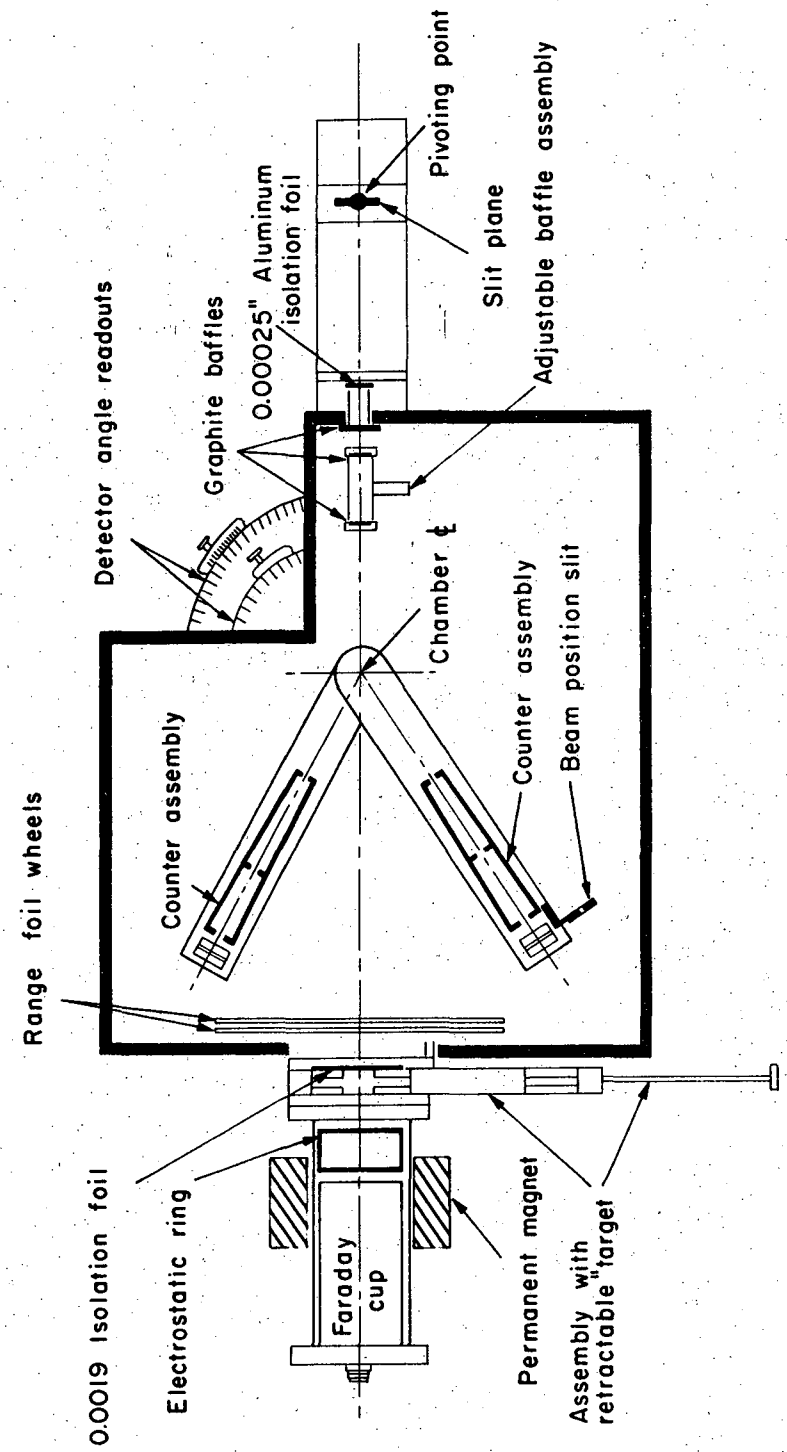
XBL685-2624
Pivoting point
Slit plane
Adjustable baffle assembly
0.00025" Aluminum isolation foil
Graphite baffles
Detector angle readouts
Chamber ℄
Counter assembly
Beam position slit
Counter assembly
Range foil wheels
0.0019 Isolation foil
Electrostatic ring
Faraday cup
Permanent magnet
Assembly with retractable "target

Fig. 1

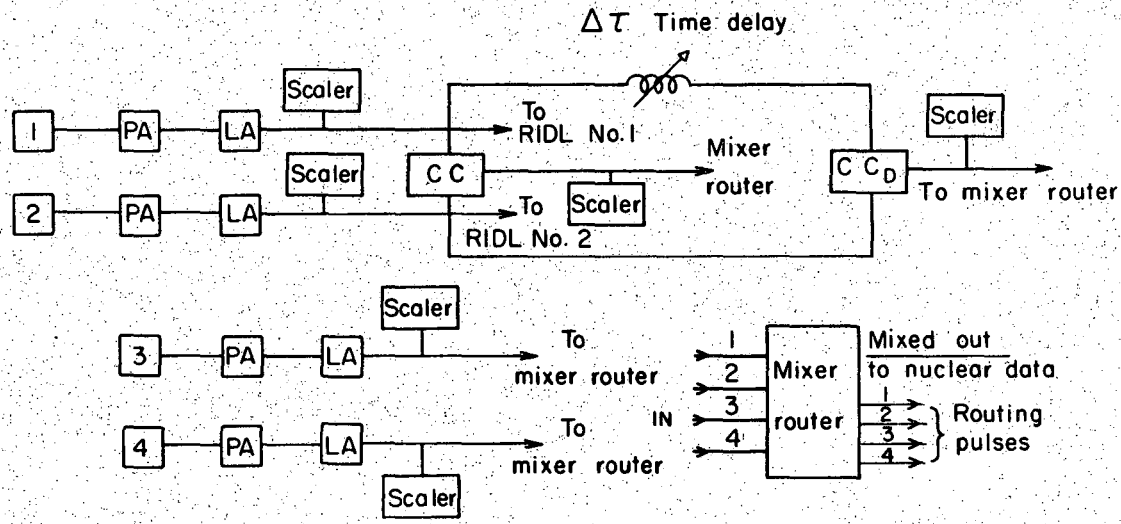
Δτ Time delay
1
PA
LA
Scaler
To RIDL No. 1
2
PA
LA
Scaler
CC
Mixer router
Scaler
To RIDL No. 2
C C$_D$
Scaler
To mixer router
3
PA
LA
Scaler
To mixer router
4
PA
LA
Scaler
To mixer router
IN
1
2
3
4
Mixer router
Mixed out to nuclear data
1
2
3
4
Routing pulses
XBL685-2619

Fig. 2

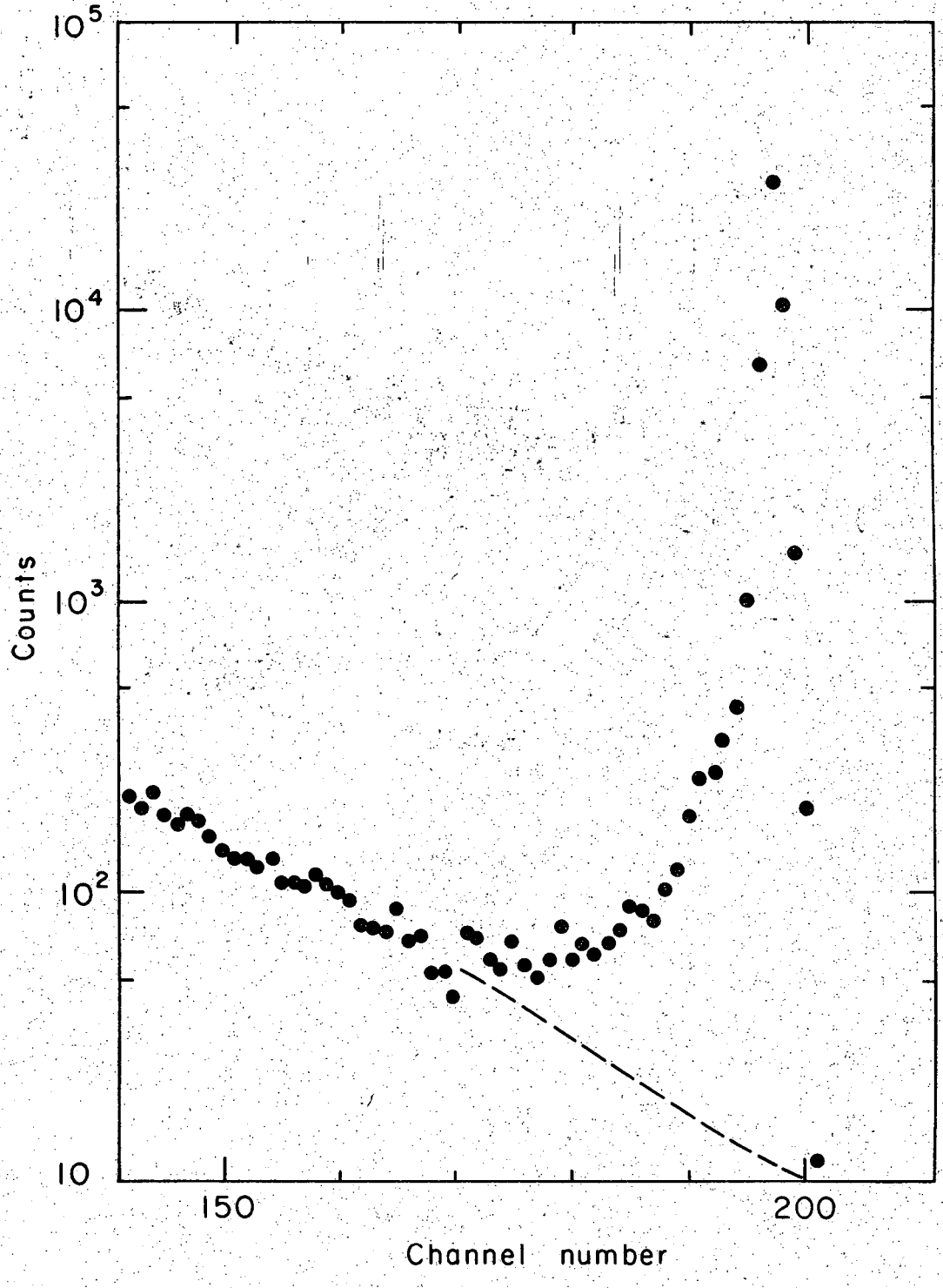

XBL 685-2757

Fig. 3

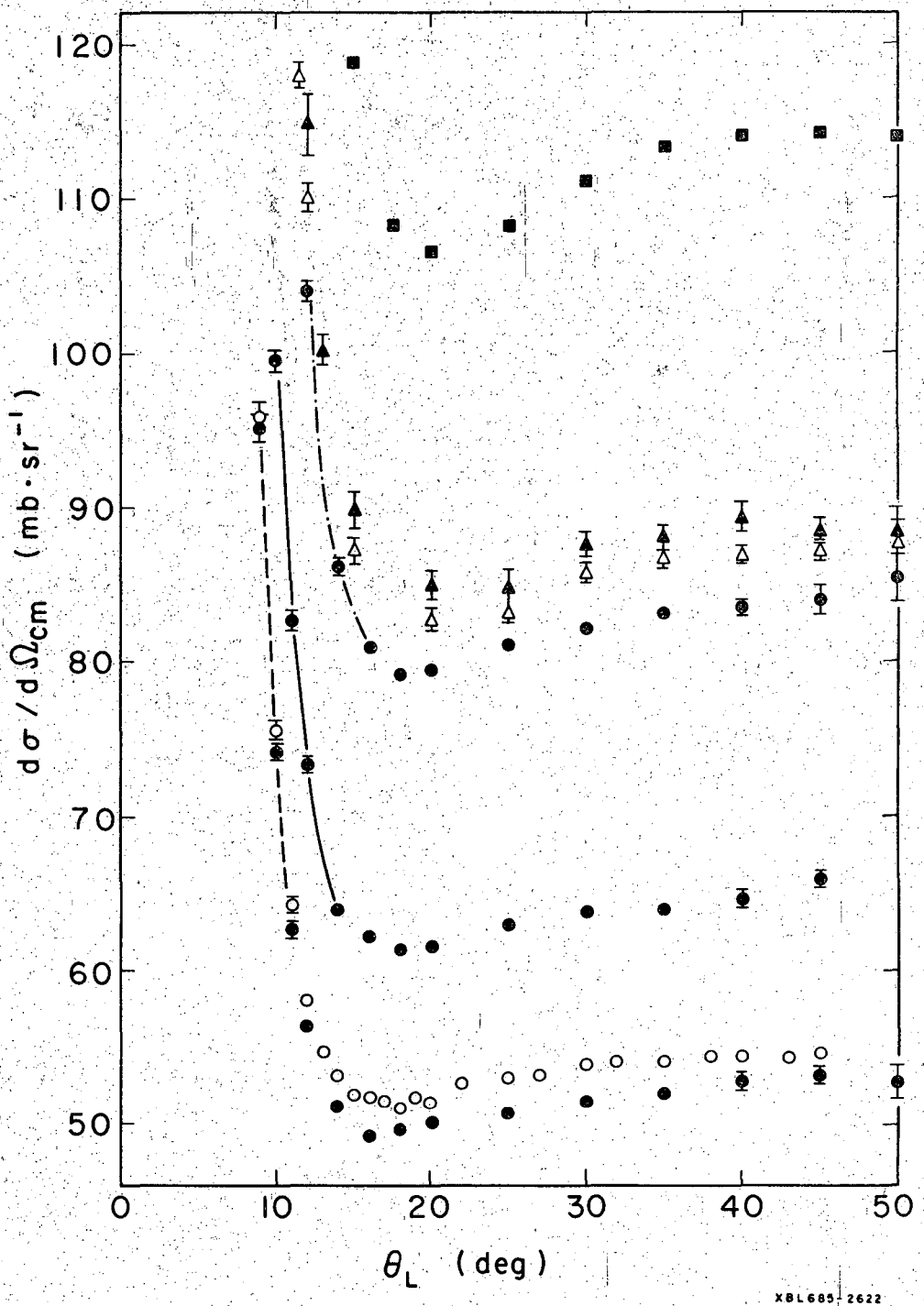
120
110
100
90
80
70
60
50
0
10
20
30
40
50
dσ / dΩcm (mb·sr⁻¹)
θL (deg)
XBL685-2622

Fig. 4

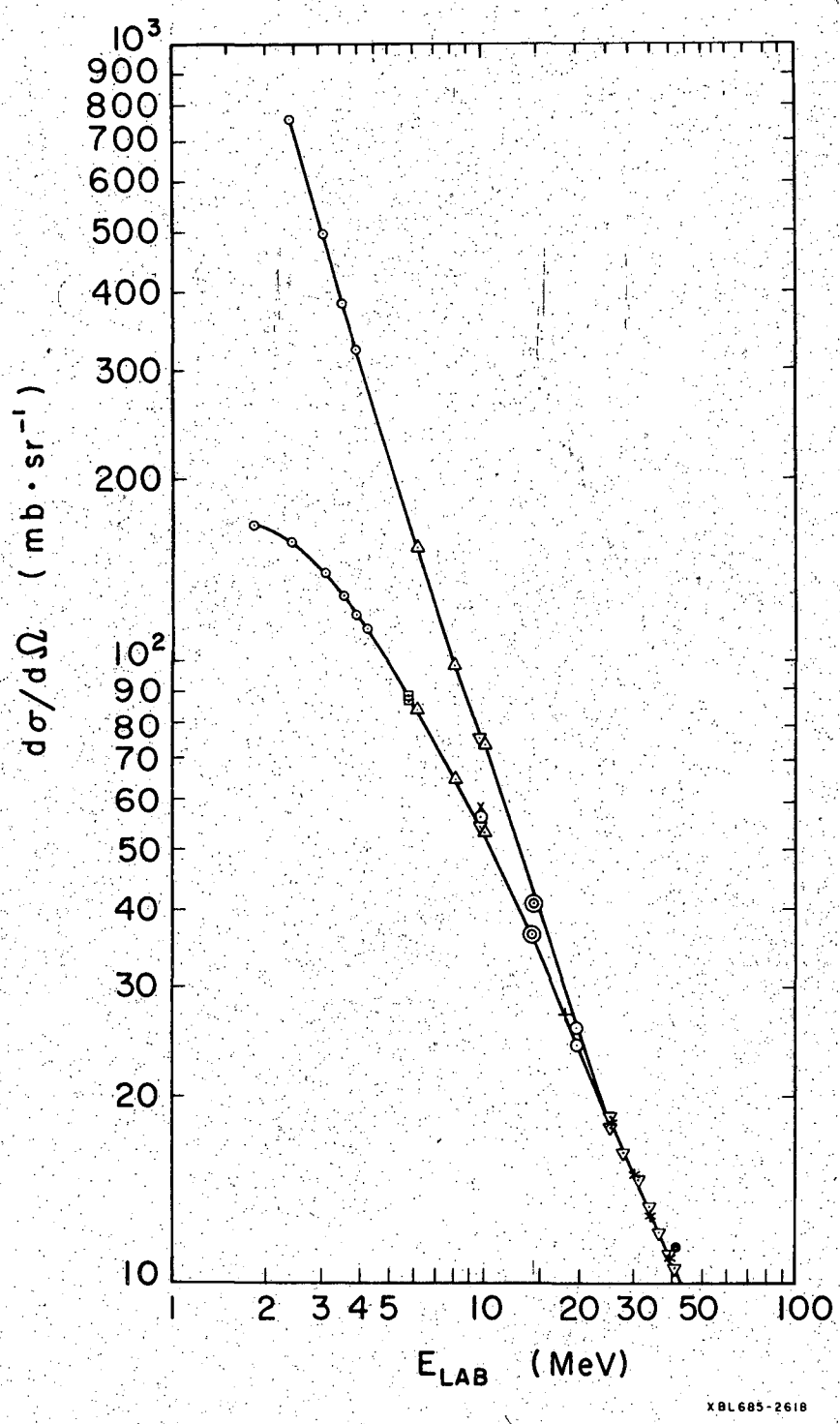
10^3
900
800
700
600
500
400
300
200
10^2
90
80
70
60
50
40
30
20
10
$d\sigma/d\Omega$ (mb · sr^{-1})
1
2
3
4
5
10
20
30
50
100
E_{LAB} (MeV)
XBL685-2618

Fig. 5

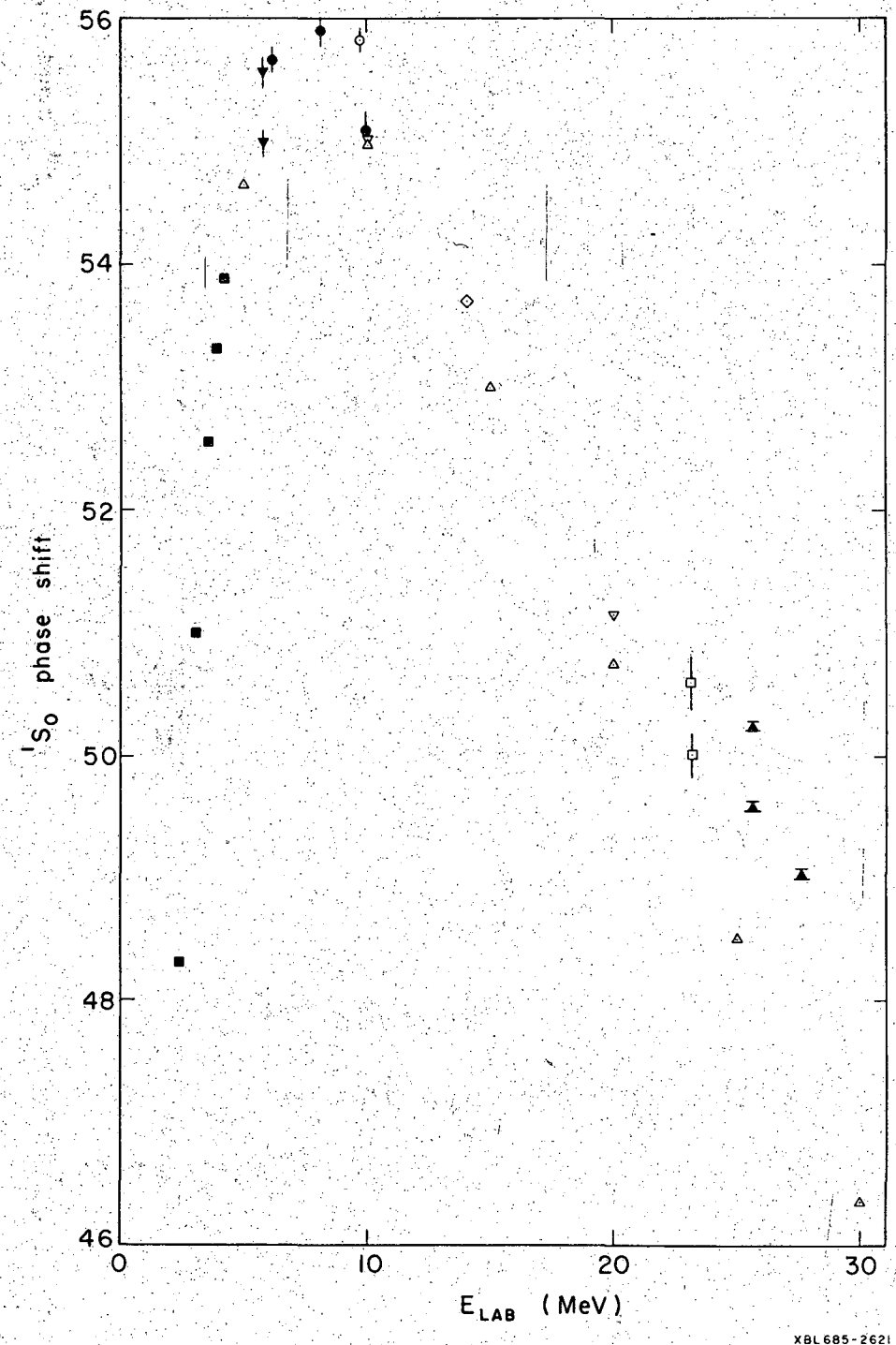

Fig. 6

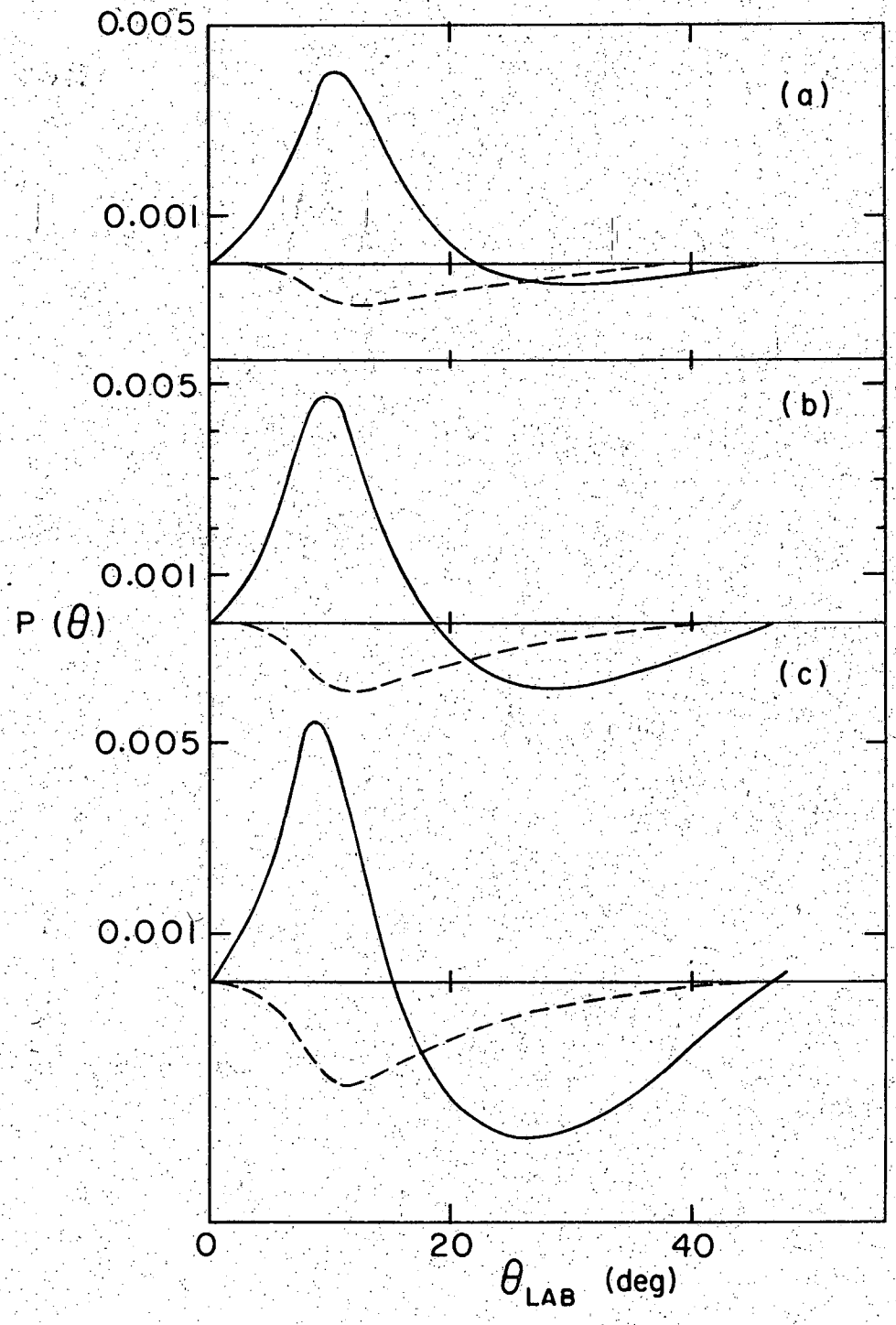
0.005
0.001
(a)
0.005
0.001
(b)
P (θ)
(c)
0.005
0.001
0
20
40
θLAB (deg)
XBL685-2620

Fig. 7